J. Fluid Mech. (2007), *vol.* 587, *pp.* 45–72.
doi:10.1017/S0022112007007276 Printed in the United Kingdom

Quasi-static rheology of foams. Part 2. Continuous shear flow

ALEXANDRE KABLA[1], JULIEN SCHEIBERT[2] AND GEORGES DEBREGEAS[2]

[1]Department of Engineering, University of Cambridge, Trumpington Street, Cambridge, CB2 1PZ, UK

[2]Laboratoire de Physique Statistique, Ecole Normale Supérieure, CNRS – UMR 8550, 24 Rue Lhomond, 75231 Paris Cedex 05, France

(Received 23 May 2006 and in revised form 29 April 2007)

The evolution of a bidimensional foam submitted to continuous quasi-static shearing is investigated both experimentally and numerically. We extract, from the images of the sheared foam, the plastic flow profiles as well as the local statistical properties of the stress field. When the imposed strain becomes larger than the yield strain, the plastic events develop large spatial and temporal correlations, and the plastic flow becomes confined to a narrow shear band. This transition and the steady-state regime of flow are investigated by first focusing on the elastic deformation produced by an elementary plastic event. This allows us to understand (i) the appearance of long-lived spatial heterogeneities of the stress field, which we believe are at the origin of the shear-banding transition, and (ii) the statistics of the dynamic fluctuations of the stress field induced by plastic rearrangements in the steady-state regime. Movies are available with the online version of the paper.

1. Introduction

As in most non-thermal disordered systems, the mechanical properties of foams are history dependent; they vary with the shear sequence which has been previously applied to the sample. In Part 1 (Kabla & Debrégeas 2007), this behaviour was evidenced using a numerical quasi-static model of a two-dimensional foam submitted to an oscillating strain of moderate amplitude (less than one). A fresh (unsheared) foam was found to exhibit a continuous change in its elastic modulus, normal stress difference and yield stress, as the number of applied shear cycles was increased. This evolution of the mechanical response was associated with a measurable modification of the foam structural properties: oscillating shear relaxes the foam structure and produces anisotropy in the film network.

When a foam is sheared beyond the plastic strain limit (of the order of 1), it flows continuously as a viscous liquid with a viscosity that decreases with the shear rate (Khan, Schnepper & Armstrong 1988). At vanishingly low shear rate however, i.e. when the typical rearrangement duration becomes smaller than the inverse of the strain rate, the flow becomes intermittent (Gopal & Durain 1995, 1999). This latter regime can be probed by performing a creep experiment in which the stress is measured while the foam is slowly driven. The resulting stress versus strain curve exhibits an initial quasi-linear part, then reaches a maximum before decaying to a lower value. In the continuous regime of flow, the stress signal exhibits large fluctuations reminiscent

of stick–slip friction which reveals the underlying intermittent nature of the plastic processes (Pratt & Dennin 2003).

Beyond these macroscopic observations, several aspects of the flow are still unclear. One of them is the existence of a quasi-static limit, a finite value of the strain rate below which the flow becomes strictly strain-rate independent. Secondly, the stability of the average flow profile with regard to shear-banding instability – i.e. the confinement of the plastic events to small regions – is still highly debated; the conditions for the appearance of shear bands remain to be clarified, even for two-dimensional foam systems (Debrégeas, Tabuteau & di Meglio 2001; Kabla & Debrégeas 2003; Cox, Weaire & Glazier 2004; Wang, Krishan & Dennin 2006; Janiaud, Weaire & Hutzler 2006).

In the present paper, the numerical model described in Kabla & Debrégeas (2007) is used and complemented by an experiment on a real bidimensionally confined aqueous foam in Couette geometry. This system allows us to measure the spatial and temporal distributions of the plastic events, as well as to monitor the evolution of the stress field as the material is continuously sheared. We attempt to correlate these two measurements in order to provide a global understanding of the elastic to plastic transition, as well as the steady-state regime of flow.

In § 2, a detailed description of the experimental and numerical systems is provided. Tests are performed to establish the existence of a quasi-static regime in the experiment, which allows for comparison with the numerical system. In § 3, the evolution of different global quantities (shear stress, free energy, flow profiles) is studied during the elastic to plastic transition. We analyse in § 4 the mechanical effect of T1 events (the elementary plastic processes in two-dimensional foams, figure 1*a*) on the stress field. Based on these results, a qualitative model is proposed that captures both the shear-banding instability and the observed heterogeneous modification of the sample structural properties (§ 5). In § 6, we investigate the dynamics of internal stress fluctuations induced by T1 events which take place in the shear band. A statistical mechanical model is proposed that accounts for most characteristics of the observed stress dynamics.

2. Experiments and simulations

2.1. *Bidimensional confined foams*

Three-dimensional foams are highly diffusive to light and thus hardly accessible to bulk imaging. Direct detection of T1 events can be obtained by diffusive wave spectroscopy (Durian, Weitz & Pine 1991; Hohler, Cohen-Addad & Hoballah 1997; Gopal & Durain 1999; Cohen-Addad, Hohler & Khidas 2004), but this technique does not provide a spatial resolution, which is why many studies on foam rheology at the bubble scale have focused on two-dimensional systems for which a direct observation is possible. Three main experimental systems have been used. (i) Langmuir foams are formed by depositing a mono-molecular layer of amphiphilic molecules on the surface of water. The monolayer exhibits a phase transition between a dense liquid phase and a dilute gas phase (Dennin & Knobler 1997; Courty *et al.* 2003). In the coexistence domain of the phase diagram, the dense and dilute regions spontaneously organize into a foam structure whose cell size is of the order of 10 μm. (ii) Rafts are made of a monolayer of soap bubbles floating at the surface of a liquid bath (Bragg & Nye 1947; Lauridsen, Twardos & Dennin 2002). The raft is sometimes covered with a transparent glass plate to facilitate its observation (Abd el Kader & Earnshaw 1999;

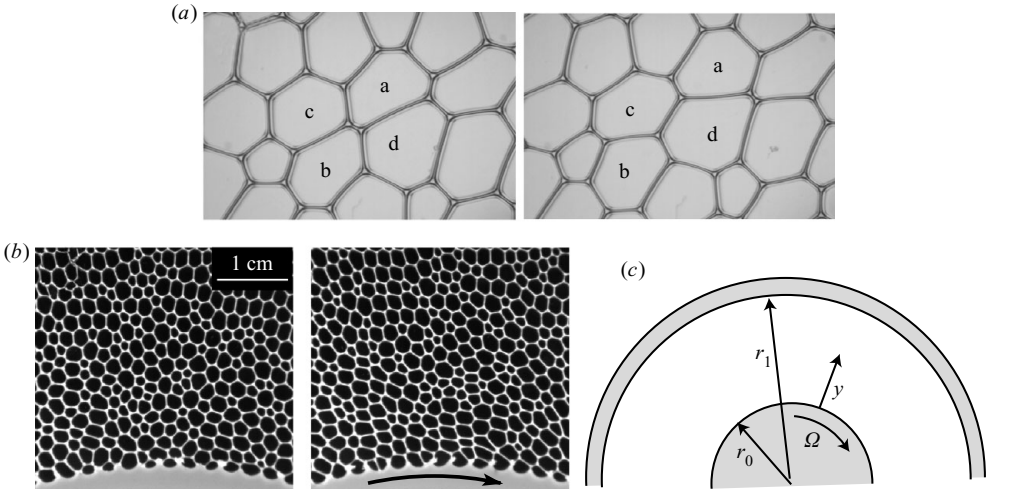

FIGURE 1. (*a*) Example of a T1 event in a two-dimensional confined foam. This elementary plastic process results from the exchange of neighbours between four adjacent bubbles (noted a, b, c and d in the pictures). (*b*) Two pictures of the confined two-dimensional foam: (i) initial (unsheared) foam, (ii) foam, under strain. (*c*) Definition of the different geometrical and kinematic parameters.

Dollet *et al.* 2005; Wang *et al.* 2006). (iii) Confined two-dimensional foams consist of an individual layer of bubbles squeezed between two flat plates (Debrégeas *et al.* 2001; Asipauskas *et al.* 2003; Cantat & Delannay 2005). The bubble diameter is adjusted so as to be larger than the distance between the plates.

In the present study, the latter configuration is used. Details of the set-up can be found in Debrégeas *et al.* (2001): it is composed of an inner shearing wheel and an outer ring (of respective radius $r_0 = 71$ mm and $r_1 = 122$ mm) confined between two transparent plates separated by a 2 mm gap. Disordered foams are obtained by bubbling nitrogen from two hoses into a controlled amount of soap solution. Here, we focus on the limit of dry (polygonal) foams with a liquid volume fraction of 1%. The mean diameter of the bubbles is of the order of 2.2 mm (figure 1). Shearing is produced by rotating the wheel with a stepper motor while the outer ring is kept fixed. Both the wheel and the ring are tooth-shaped to avoid bubble slippage. A CCD camera is positioned above the cell to allow monitoring of the foam during the experiment. The network of films is then extracted by image analysis using the software IDL.

This confined system has several important characteristics in comparison to the two other systems. First, confinement walls eliminate the effect of gas diffusion between bubbles and the external reservoir, which allows experiments to be run for about 2 h without significant change in the bubble volumes. Secondly, although this configuration avoids the dynamic coupling that occurs between the sub-phase and the foam under shear, the confinement plates introduce a viscous stress as detailed further. Lastly, the confined geometry allows access to the stress field in the material through a simple observation of the structure of the films. Since the area of the gas/liquid interface is fixed in the horizontal plane, the free energy F of any sub-volume $\mathscr{D}$ of the foam is given, to a constant, by the total area of the films that separates neighbouring

bubbles. In the limit of an infinitely dry foam, the free energy is

$$F(\mathscr{D}) = 2\Gamma h \sum_{\{\text{films inside } \mathscr{D}\}} l_i, \tag{2.1}$$

where Γ is the surface tension at the air–water interface and h is the distance between the glass plates. The sum is performed over all the films inside the sub-volume $\mathscr{D}$, and l_i are the horizontal arclengths of the films. From this expression, we introduce the line tension γ defined as: $\gamma = 2\Gamma h$. Consistently, the internal capillary stress in the confinement plane can also be extracted from the projected film network (Kraynik, Reinelt & van Swol 2003):

$$\sigma_{xy}(\mathscr{D}) = \frac{\gamma}{A(\mathscr{D})} \sum_{\{\text{films inside } \mathscr{D}\}} \frac{l_{i,x}\, l_{i,y}}{l_i}. \tag{2.2}$$

It should be noted that these two relationships are not valid *a priori* for rafts in which bubbles can deform in the vertical direction to accommodate the horizontal stress.

2.2. *The quasi-static regime of flow*

The main limitation of this experimental system is due to the viscous stress exerted on the foam by the confining walls upon shearing. Although the glass plates remain entirely wet, the motion of the soap films induces liquid flows in the plateau borders that connect the films to the plates. This yields a net viscous force that can overcome the internal friction between bubbles (Cantat & Delannay 2005). As a model of foam bulk rheology, this system is thus only valuable in the limit of quasi-static flow. This regime is expected when the shearing time scale $\tau_{shear} = \dot{\varepsilon}^{-1}$ is shorter than the time scale for stress relaxation τ_{relax} associated with a plastic event. (For consistency with the companion paper, and to avoid any confusion with the line tension γ, the shear strain will be systematically notated ε.) The flow then consists of a series of elastic charges interrupted by stress drops associated with the (rapid) plastic events (Pratt & Dennin 2003). During the charge periods, the foam is in static equilibrium, whereas all dissipative processes take place during the fast rearrangement events.

Measurements of the time τ_{relax} in confined foams have recently been carried out by Durand & Stone (2006) who showed that this time scale is mostly controlled by the surface rheology of the surfactant monolayers. For bubbles of roughly the same diameters as in the present experiment, they found that τ_{relax} is between 0.5 and 3.7 s for a large range of surface and bulk viscosities. The foaming solution used here is a commercial foaming agent (Teepol) 2% volume in water. Although it is different from what was used by Durand & Stone, 1 s can be taken as a realistic estimation of τ_{relax} for this experiment.

In order to determine the limiting rotation rate Ω for which the flow is quasi-static, several tests are carried out. For different value of Ω, we monitor the bubble displacements during the time period $\tau_0 = D/(r_0\Omega)$ required for the wheel edge to move over one mean bubble diameter D. These kinematic measurements are performed in the steady-state regime of flow which is found to be reached after the wheel has been rotated one full turn. Averages are calculated over the time and the angular coordinate. We thus extract the average displacement $u_{\parallel}(y)$ in the direction of the flow and the standard deviation of the radial displacement $\sqrt{\langle u_{\perp}(y)^2 \rangle}$ as a function of the distance y from the edge. Both quantities are scaled by the bubble diameter D.

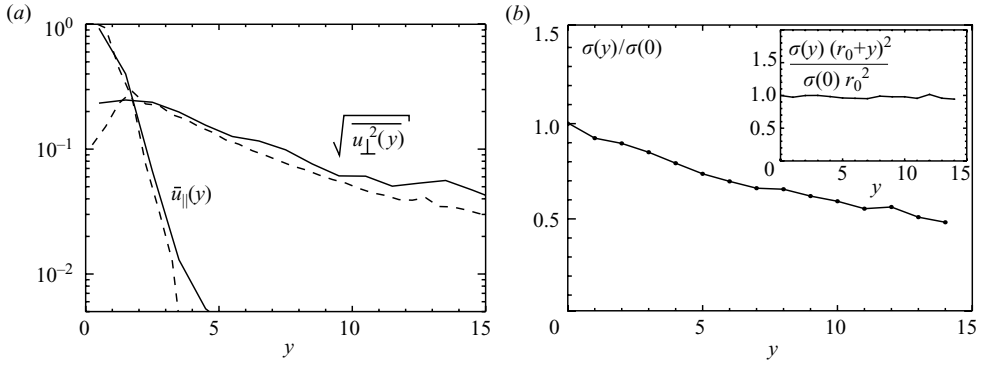

FIGURE 2. (*a*) Shear velocity profiles $u_\parallel(y)$ and transverse fluctuations profiles $\sqrt{\langle u_\perp(y)^2\rangle}$ for different rotation rates $\Omega = 2.9 \times 10^{-3}\,\mathrm{rad\,s^{-1}}$ (solid line) and $\Omega = 5.8 \times 10^{-3}\,\mathrm{rad\,s^{-1}}$ (dashed line) (data from the experiment). These measurements are obtained by averaging displacements over time and the angular coordinate. The radial displacements are obtained by tracking the bubbles over a time τ_0 corresponding to a displacement of the inner wheel equal to a bubble diameter D. (*b*) The shear stress profile as a function of the distance from the inner wall. The inset demonstrates that this profile is consistent with the expected stress decay in Couette geometry (equation (2.3)).

Figure 2(*a*) shows the resulting profiles for two different rotation rates $\Omega = 2.9 \times 10^{-3}$ and $5.8 \times 10^{-3}\,\mathrm{rad\,s^{-1}}$. The plastic flow is mostly confined in a small region – the so-called shear–band in the vicinity of the wheel edge. The average flow profile $u_\parallel(y)$ exhibits an exponential decay from the wheel edge towards the outer ring. The decay length is approximately one bubble diameter (Debregeas *et al.* 2001) so that the maximum local shear rate is of the order of $\dot{\varepsilon}_{max} \sim \Omega r_0/D$.

Although the mean displacement in the shear direction is barely measurable beyond the fifth row of bubbles, the standard deviation of the transverse displacements remains large all across the gap. These latter are a signature of the long-range elastic deformations induced by plastic events in the shear band (see § 6). The similarity of the curves for the two different rotation rates establishes that the dynamic is quasi-static. In this regime, the only relevant parameter is the total imposed strain and not the shear rate. Hereinafter, all the experiments are performed at the same rotation rate which is set at $\Omega = 2.9 \times 10^{-3}\,\mathrm{rad\,s^{-1}}$, corresponding to $\dot{\varepsilon}_{max} = 0.1\,\mathrm{s^{-1}}$. (It should be noted that, for larger rotation rates, a rapid decrease in the amplitude of the transverse fluctuations is observed, although the shear profile remains mainly unchanged. This indicates that the independence of the average shear profile with the imposed shear rate is not a sufficient criterium to establish that the flow is quasi-static.)

A further test that the flow is quasi-static at this shear rate is carried on through a mechanical approach. In order to demonstrate that the viscous stress due to the confining wall is negligible, as expected in the quasi-static regime, we check that the only contribution to the internal stress is due to surface tension. Using (2.2), the average shear stress profile along the radial direction is measured (figure 2*b*). It appears to follow the expected decay for a cylindrical Couette geometry:

$$\sigma_{xy}(y) = \sigma_{xy}(y=0)\,\left(\frac{r_0}{r_0+y}\right)^2. \tag{2.3}$$

These different tests establish that, within the resolution in stress and displacement measurements, no observable shear-rate dependence pertains in this slow shear-rate

regime. Still, at any finite shear rate, a velocity dependent drag force of the bubbles on the confining plates is still present. Janiaud and colleagues argue that this residual force, however small, is responsible for the observed shear-banding instability (Clancy *et al.* 2006; Janiaud, Weaire & Hutzler 2006). These papers were motivated by an experimental study in which Wang *et al.* (2006) compared the flow profiles in plane parallel geometry for bubble rafts with and without covers. In the first configuration, they observed an exponential decay of the bubble velocity, whereas in the second situation they found a linear velocity profile.

In order to describe the flow profile $v(y)$ in confined geometry, Janiaud *et al.* start from the standard Bingham rheological equation, $\sigma = \sigma_y + \eta \partial v/\partial y$. The friction force on the confining plates is postulated to be proportional to the local velocity $v(y)$ and characterized by a drag coefficient β. This leads to an expression of the stress gradient, $\partial\sigma/\partial y = \eta \partial^2 v/\partial y^2 + \beta v$. In the steady-state regime, the mechanical equilibrium imposes $\partial\sigma/\partial y = 0$ which yields an exponential decay of the velocity profile with a decay length equal to $(\beta/\eta)^{1/2}$. It should be noted that this result is also expected for a Newtonian viscous fluid sheared horizontally in a confined (Hele-Shaw) geometry.

This model is based on a continuous description of the foam and thus ignores any heterogeneity in the stress associated with the granularity of the material. This might be questionable for systems which exhibit yield stress and are thus critically unstable at the threshold of flow. In our situation, i.e. for polydisperse foams, the static stress heterogeneity over a few bubbles is of the order of the plastic yield stress itself (see later in this paper and in Kabla & Debrégeas 2003). By comparison, the drag force is not measurable, so at least one to two orders of magnitude smaller. Our approach in the present paper is therefore the reverse of Janiaud's: it explicitly takes into account the stress heterogeneity due to the cellular nature of the material, but neglects the (non-measurable) viscous drag.

2.3. *Numerical model*

From (2.1), it appears that the static equilibrium configuration of the foam corresponds to a minimum of the total length of the (projected) two-dimensional film network, with the constraint of a fixed bubble area. This is precisely the basis of the quasi-static simulation, described in Part 1, which therefore provides a realistic numerical counterpart to this set-up.

Kabla & Debrégeas (2003) showed that the numerical foam exhibits a shear-banding instability whose characteristics (flow profiles, velocity fluctuations, ...) are similar to those observed in the experimental system (Debrégeas *et al.* 2001). One may argue that the shear banding observed in the experiment simply results from the fact that a foam is a yield stress fluid. For such a material, the decay of the imposed stress associated with the Couette geometry (see (2.3)) leads to a confinement of the flow within a small region near the inner wall. However, the numerical simulations are performed in plane parallel geometry for which the shear stress is homogeneous across the gap, suggesting that the localization process, in this case, has a different origin.

In the present paper, we combine the two systems to study in detail the elastic to plastic transition as well as the dynamics of local stress fluctuations in the steady-state regime of flow. The numerical procedure for the evolution of the foam under shear, and the definition of the different quantities monitored, are similar to those described in Part 1. The dimension of the numerical foam in the shear direction is increased in order to limit non-physical correlations induced by the periodicity. The

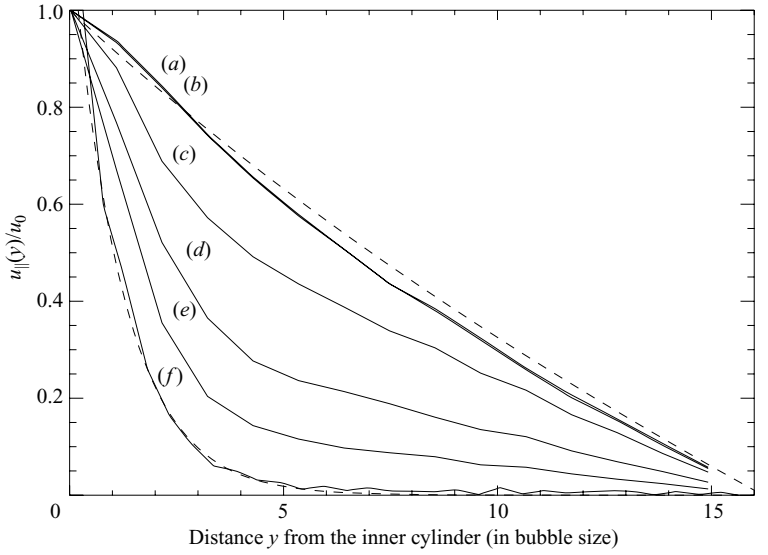

FIGURE 3. Transition from the purely elastic response to localized flow (experiment). The averaged displacement profile is plotted for different imposed strains: (*a*) $0 < \overline{\varepsilon} < 0.125$, (*b*) $0 < \overline{\varepsilon} < 0.25$, (*c*) $0 < \overline{\varepsilon} < 0.5$, (*d*) $0 < \overline{\varepsilon} < 1$, (*e*) $0 < \overline{\varepsilon} < 0.2$, (*f*) $2 < \overline{\varepsilon} < 8$. The curves (*a*) and (*b*), which almost overlap, correspond to the expected response of an elastic material (dashed line $u_{\parallel}(y) = u_0((y + r_0)/r_2 - r_2/(y + r_0))/(r_1/r_2 - r_2/r_1)$ with $r_2/r = 1.5$). The profile in steady-state regime (*f*) is fitted by an exponential: $u(y) = u_0 \exp(-y/1.2)$.

numerical foam dimension is thus 40×16 bubbles. When possible, results from both the experiment and the simulation are presented. However, because of the limited resolution of the experiment, some measurements can be obtained only with the numerical system.

3. Transition to shear banding

In order to examine the transition to shear banding, an experiment is performed in which the wheel is first rotated counterclockwise one full turn. The evolution of the foam is then monitored as the wheel is rotated backwards. Figure 3 shows the modification of the displacement profiles in the shear direction $u_{\parallel}(y)$ as the imposed deformation is increased from 0 to 2, as well as the corresponding profile in the steady-state regime. All distances are scaled with the displacement u_0 of the wheel edge during the same period. For small imposed strain ($\epsilon \sim 0.25$), the foam deforms almost elastically (few T1 events occur). The corresponding profile is consistent with what is expected for a linear elastic deformation in Couette geometry:

$$u_{\parallel}(y) = u_0 \frac{(y + r_0)/r_1 - r_1/(y + r_0)}{r_0/r_1 - r_1/r_0}, \tag{3.1}$$

where r_0 and r_1 are the inner and outer diameters, respectively. Beyond $\varepsilon \sim 0.25$, strain starts to localize in a shear band. For $\varepsilon \geqslant 1$, the flow has reached its steady-state regime and the flow profile exhibits an exponential decay: $u_{\parallel}(y) = u_0 \exp(-y/\lambda)$, with $\lambda \sim 1.2$.

In the experiment, the introduction of the foam in the gap involves the shearing of the material in a poorly controlled way. The numerical simulation is therefore more adequate for probing the transient regime of shear which strongly depends on the

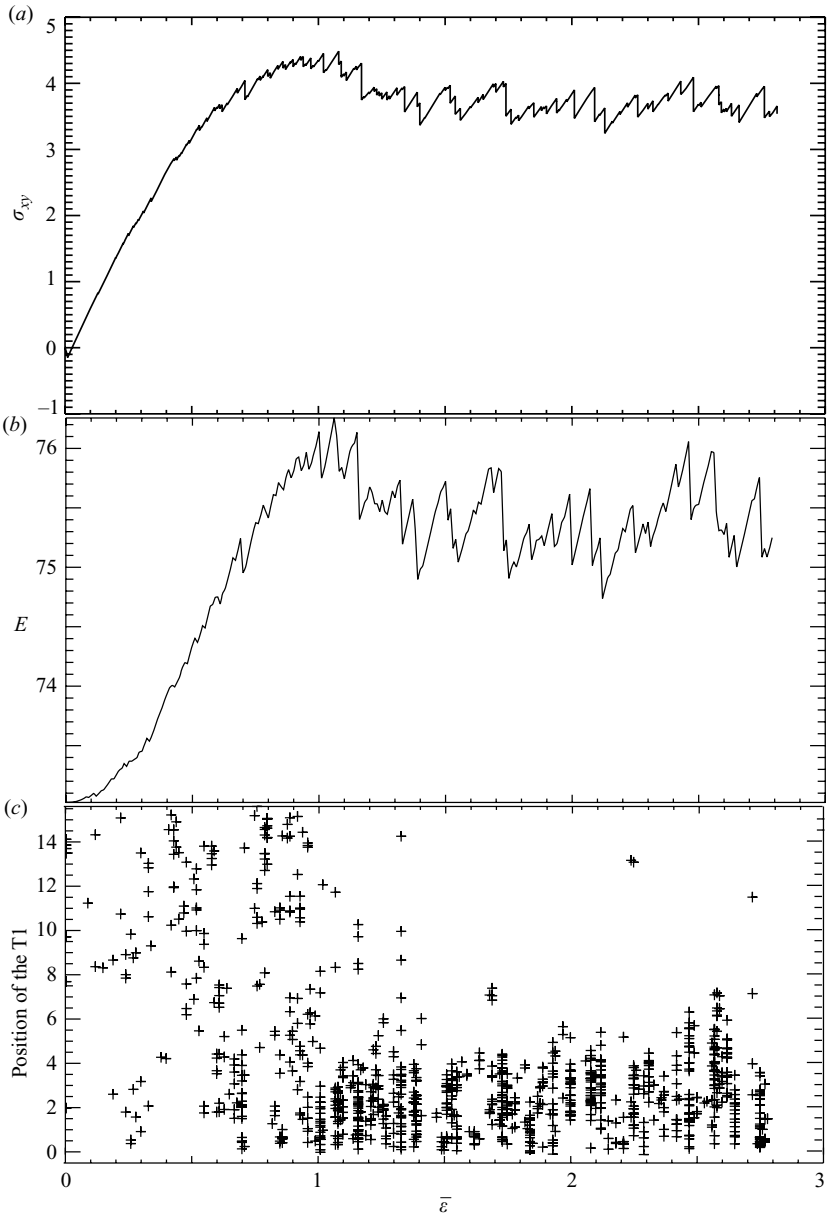

FIGURE 4. Evolutions of (*a*) the shear stress, (*b*) the free (line-length) energy and (*c*) the positions of the T1 events within the gap as a function of the applied strain $\overline{\epsilon}$ (data from the simulation).

shear history of the sample. Figure 4 shows, as a function of the wall displacement, the evolution of the mean shear stress, the energy of the foam (total film length), and the location of the T1 events across the gap. The line tension is set at 1, and the foam dimensions are set at $L_x \times L_y = 2.5 \times 1$; the wall displacement d is thus numerically equivalent to the total applied strain $\overline{\varepsilon} = d/L_y$. For $\overline{\varepsilon} < 1$, the deformation of the material is mostly elastic: only a small number of T1 events, uniformly distributed across the gap, are observed. For $\overline{\varepsilon} \sim 1$, shear-banding occurs: most of the T1 events

gather in a narrow region close to one of the confining walls (the movie of this simulation is available with the online version of the paper). The sharp transition is associated with an overshoot of the shear stress and the appearance of large avalanches of rearrangements, as evidenced by the increase of the drop amplitudes in the shear stress and energy curves (figure 4*a*, *b*).

As the foam is sheared, it experiences a series of plastic events that modify its topological structure. Each metastable configuration is entirely characterized by the relative positions of the bubbles. We showed in Part 1 that this trajectory in the configuration space can be associated with a path in an energy landscape. After each T1 event, the system falls into a new energy basin which is defined as the energy versus strain relation of the given structure.

For each value of the total imposed strain $\overline{\varepsilon}$, this quadratic function can be numerically obtained using the following method (detailed in Part 1): after an imposed strain $\overline{\varepsilon}$, the possibility for T1 events to occur is forbidden in the simulation so that the topology is frozen in its particular configuration. The line-length energy of the foam $E(\varepsilon')$ is then monitored as a function of the strain ε' and the resulting curve is fitted using the following relation:

$$E_{elast}(\varepsilon') = E_0(\overline{\varepsilon}) + \tfrac{1}{2}A\mu(\overline{\varepsilon})\,(\varepsilon' - \varepsilon_{plast}(\overline{\varepsilon}))^2, \tag{3.2}$$

where A is the total area of the foam. This allows us to extract, for each configuration reached after an imposed strain $\overline{\varepsilon}$, several parameters that define the energy basin: E_0 is the minimum energy of the structure, μ is the tangent shear modulus along the x-direction and ε_{plast} is the value of the shear strain (or equivalently the position of the wall) for which the foam energy is minimum. The latter can be viewed as the amount of strain that has been irreversibly released through the successive plastic events that have occurred since the shear started. The imposed strain can thus be decomposed into an irreversible (plastic) and a stored (elastic) component: $\overline{\varepsilon} = \varepsilon_{elast} + \varepsilon_{plast}$.

Figure 5 shows the evolution of these different numbers as a function of the imposed strain $\overline{\varepsilon}$. In agreement with the findings of Part 1, E_0 and μ are found to decrease with the strain for $\overline{\varepsilon} < 0.5$. In this transient regime, ε_{plast} remains almost constant which indicates that the initial T1 events relax the structure, but do not significantly release the shear strain. As the system enters the localized regime, a significant increase of E_0 is observed whereas μ remains unchanged. The plastic component of the strain ε_{plast} linearly increases whereas the elastic part reaches a constant value. In the steady-state regime, the T1 events mainly release the imposed strain.

3.1. *Discussion*

In the numerical simulation, although the imposed stress is uniform, the flow is highly asymmetrical. As already pointed out by Kabla & Debrégeas (2003) and Varnik *et al.* (2003), this observation hampers the possibility of describing the foam mechanical response using a rheological equation such as $\sigma = f(\dot{\epsilon})$. In particular, the Hershel–Buckley model, $\sigma = \sigma_0 + \mu\dot{\epsilon}^n$, which is commonly used for aqueous foams, is expected to fail in the limit of $\dot{\epsilon} = 0$. This has been established by Rodts, Baudez & Coussot (2005) using MRI imaging of three-dimensional foams sheared in a Couette cell. They observe a discontinuous drop of the shear rate measured across the gap, from $\dot{\epsilon}_c = 10\,\mathrm{s}^{-1}$ to 0. The width of the transition zone, which is below the MRI resolution, is believed to be of the order of a few bubble diameters.

This observation can be understood by noting that $\dot{\epsilon}_c^{-1} = 0.1\,\mathrm{s}$ is of the order of the duration of a T1 event which has been evaluated for the same commercial shaving foam by Gopal & Durian (1999). When the average strain rate falls below this critical

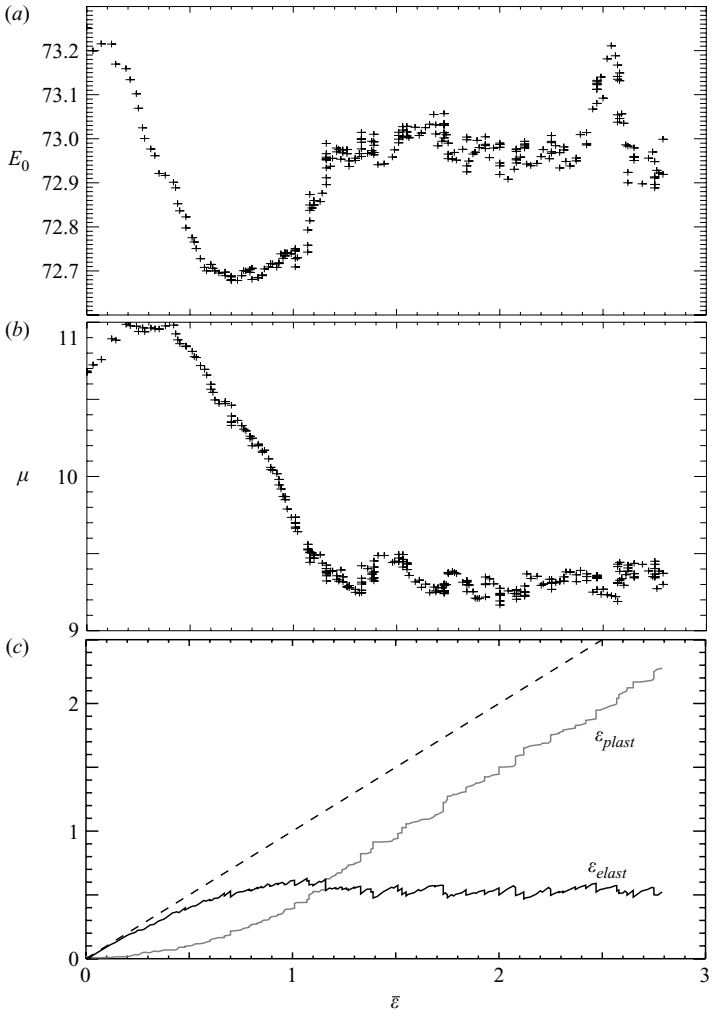

FIGURE 5. Evolutions of (*a*) the structural energy E_0, (*b*) the shear modulus, and (*c*) the plastically relaxed and elastically stored strain components as a function of the imposed strain (data from the simulation). In (*c*), the dashed line is the sum of the two components of strain which, by definition, is equal to the imposed strain.

value, the flow becomes intermittent: the local instantaneous strain rate is either 0 in the absence of a T1 process, or $\dot{\epsilon}_c = 1/\tau_{T1}$ when a T1 occurs. In this regime, the long-range elastic stress that couples the different regions of the material becomes dominant over local viscous stress and allows for spatially heterogeneous flow to develop. In the case of Rodts' experiment, as well as in our system, this leads to an abrupt decay of the plastic strain rate over a distance of a few bubble diameters.

In order to understand the spatial and temporal statistics of the plastic processes in the intermittent regime, we must probe the elastic effect of the plastic events on the entire material. This is done in the next section using the results of the numerical simulation which, in contrast to the experiment, provides a sufficient resolution for such a study.

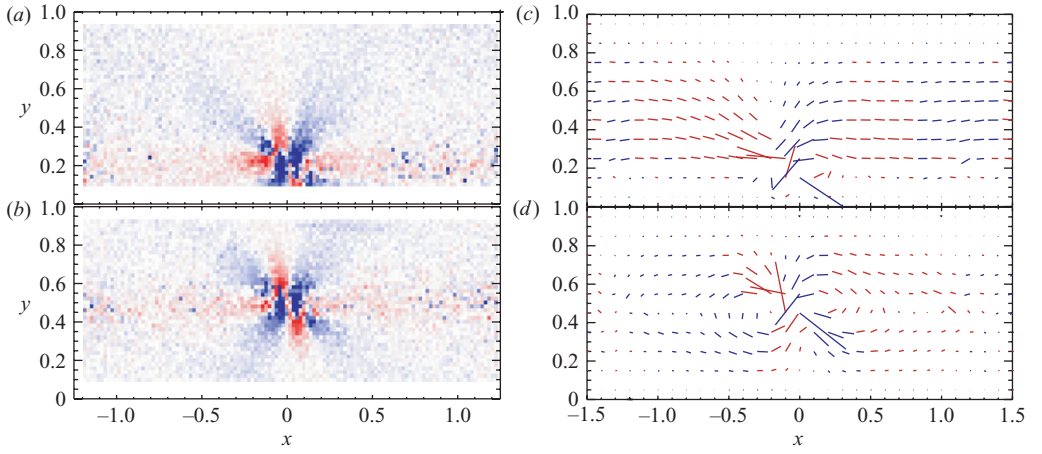

FIGURE 6. (a, b) Shear stress variation and (c, d) displacement fields induced by a T1 event, respectively, located close to the wall and in the middle of the gap. These simulation data have been obtained by averaging 100 different T1 events located at the same distance from the wall. In (a) and (b), blue corresponds to a stress decrease (with respect to the imposed stress), and red to a stress increase.

4. The short-time scale: T1 events and avalanches

4.1. *Elastic effect of a T1 event*

The stress field in the foam can be evaluated by extrapolating (2.2) to small sub-regions (in practice down to the bubble size). By comparing the equilibrated structures of the foam before and after a rearrangement, we can extract the local displacement and shear stress variation induced by the event at each location. Figure 6 displays the resulting fields for a T1 event located in the middle of the foam and close to one of the walls. In order to enhance the resolution of the measurements, the data are averaged over one hundred T1 events located at the same distance from the wall.

Analytical results of Picard *et al.* (2004) show that this propagator corresponds to the response of a two-dimensional elastic material to an elementary force quadrupole. It should be stressed, however, that the T1 propagator obtained from the simulation is slightly asymmetrical which might be due to the shear-induced anisotropy of the foam.

We first focus on the line-averaged (along the shear direction x) characteristics of these fields. The average shear stress relaxation is found to be identical for each line as imposed by the constraint of mechanical equilibrium. Figures 7(a) and 7(b) show the displacement profiles; to first order, a T1 event is equivalent to a fracture running along the line of the T1 event. The upper part of the material 'slides' with respect to the lower part over a length δd_{T1}. In each sliding block, the displacement profile is linear and the slope defines a shear strain $\delta\varepsilon_{T1} = \delta d_{T1}/L_y$ where L_y is the gap width.

Because of the foam polydispersity, a 30% dispersion in the measured value of δd_{T1} is observed. A scaling of the mean length δd_{T1} can be estimated by considering that the bubbles involved in the T1 event move over a distance of order D, whereas the L_x/D bubbles in the rest of the line do not rearrange (L_x is the size of the foam in the shear direction). Thus the average sliding distance δd_{T1} is expected to be

$$\delta d_{T1} \approx D \cdot \frac{D}{L_x}. \tag{4.1}$$

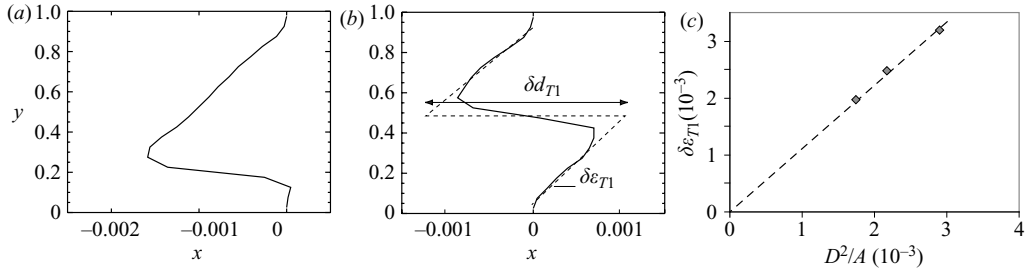

FIGURE 7. (a, b) The deformation profiles (x-averaged displacement) induced by a T1 event located (a) near the wall and (b) in the middle of the gap. δd_{T1} is the mean sliding distance, and $\delta\varepsilon_{T1}$ the corresponding elementary strain release induced by the T1 event. Because of the foam polydispersity, a 30% dispersion in the these quantities is observed. (c) Dependence of $\delta\varepsilon_{T1}$ on the system size (D is the mean bubble diameter and A is the foam area). Each data point corresponds to an average over 100 T1 events.

The elastic deformation released by the T1 event is thus

$$\delta\epsilon_{T1} = \frac{\delta d_{T1}}{L_y} = \frac{D^2}{A}, \tag{4.2}$$

where A is the total area of the foam. These two relations are successfully confirmed by varying the system size (figure 7c).

Having identified the result of a single T1 event, the cumulative effect of a series of these plastic events on the evolution of the stress field can now be examined. As previously, we consider a system of size (Lx, Ly), sheared along the x-direction, with an imposed shear rate $\dot{\bar{\varepsilon}}$ in the quasi-static regime. We denote $u_{\parallel}(y, t)$ the displacement in the x-direction at a distance y from the wall, averaged over the shear direction. The associated strain $\varepsilon(y, t) = \mathrm{d}u_{\parallel}/\mathrm{d}y$ is decomposed into a (stored) elastic term $\varepsilon_{elast}(y, t)$ and a plastic term $\varepsilon_{plast}(y, t)$:

$$\varepsilon(y, t) = \varepsilon_{elast}(y, t) + \varepsilon_{plast}(y, t). \tag{4.3}$$

We now define $\omega(y, t)$ as the density function of T1 events occurring at a time t and a height y in the foam:

$$\omega(y, t) = \sum_{\mathrm{T1}\,(i)} \delta(y - y_{T1(i)}) \cdot \delta(t - t_i). \tag{4.4}$$

When a rearrangement occurs at a location y_{T1}, it increases the plastic strain by a quantity δd_{T1} at $y = y_{T1}$, and elastically relaxes the entire system by a strain amplitude $\delta\epsilon_{T1} = \delta d_{T1}/L_y$. We can thus write:

$$\frac{\partial\, \varepsilon_{elast}(y, t)}{\partial t} = \dot{\bar{\varepsilon}} - \delta\varepsilon_{T1} \int_y \omega(y', t)\, \mathrm{d}y', \tag{4.5}$$

$$\frac{\partial\, \varepsilon_{plast}(y, t)}{\partial t} = \omega(y, t)\, \delta d_{T1}. \tag{4.6}$$

The integral in (4.5) is a direct consequence of the long-range elastic effect of T1 events. The strain evolution at any location in the foam depends on all the rearrangements occurring in the system. Moreover, $\varepsilon_{elast}(y, t)$ does not depend on y; as the local shear stress is uniform in all the lines, the elastically stored deformation also remains uniform. These equations yield a relationship between the statistics of

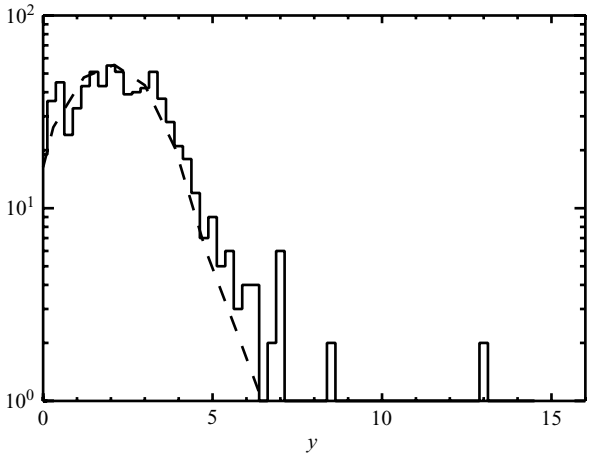

FIGURE 8. Gradient of the flow profile and frequency of the T1 events for each line (simulation). The coordinate y is expressed in bubble diameter D. —, histogram of T1 positions; - - -, gradient of the velocity profile.

the plastic events and the flow profile $v(y) = \mathrm{d}u_{\parallel}/\mathrm{d}t$ in the steady-state regime:

$$\frac{\mathrm{d}v(y)}{\mathrm{d}y} = \left\langle \frac{\partial\, \varepsilon(y,t)}{\partial t} \right\rangle_t = \underbrace{\left\langle \frac{\partial\, \varepsilon_{elast}(y,t)}{\partial t} \right\rangle_t}_{=0} + \left\langle \frac{\partial\, \varepsilon_{plast}(y,t)}{\partial t} \right\rangle_t, \tag{4.7}$$

$$\Rightarrow \frac{\mathrm{d}v(y)}{\mathrm{d}y} = \langle \omega(y,t) \rangle_t\, \delta d_{T1}. \tag{4.8}$$

This relation is demonstrated in figure 8 which displays both the gradient of the flow profile and the histogram of the T1 event locations in the steady-state regime. This result is due to the foam elasticity which induces global shear stress relaxation in response to local plastic events. This effect allows for the existence of heterogeneous flow profiles. More precisely, this approach shows that any flow profile is consistent with the mechanical equilibrium condition, as each T1 event produces the same stress relaxation in each line, regardless of its location in the gap. Therefore, this line-averaged description appears inadequate to address the question of the shear-banding instability and further examination into the origins of the spatial correlations between T1 events is required.

4.2. *From a T1 event to the avalanche*

When a T1 event occurs, it generally triggers an avalanche of events that take place in the neighbouring region. Figure 9(*a*) shows the distribution of avalanche sizes measured in numbers of T1 events in the simulation. A power-law decay of the avalanche size distribution is observed, with an exponent -1.5 consistent with numerical studies on elastic disordered systems (Chen, Bak & Obukhov 1991; Okuzono & Kawasaki 1995). As shown in figure 9(*b*), the energy released during the avalanche is a linear function of the avalanche size: each rearrangement releases a given amount of energy (or shear stress) which numerically coincides with $A\, \delta\varepsilon_{T_1}\, \overline{\sigma_{xy}}$. Though the quasi-static model used here is *a priori* inaccurate for modelling fast avalanching processes, it agrees with the vertex model (Okuzono & Kawasaki 1995) which includes viscous dissipation at the bubble scale; this suggests that the exponent

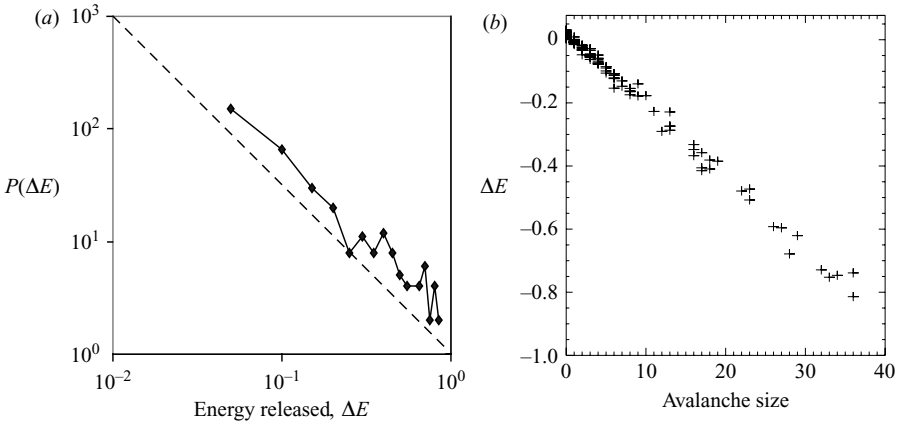

FIGURE 9. (*a*) Statistical distribution of the elastic energy released by the avalanches of plastic events. The dashed line indicates a −1.5 exponent power-law decay. (*b*) Released energy as a function of the number of T1 events involved. These results come from the simulation data in the steady-state regime.

value is likely to be a generic feature of these systems. This observation contrasts, however, with the measurements of Tewari *et al.* (1999) who observe with a bubble model (Durian 1995) a weaker power law for the rearrangement energy histograms, as well as a nonlinearity between the energy released per avalanche and the avalanche size. This discrepancy might result from the different nature of the plasticity between the vertex model and the bubble model where bubbles are modelled as soft overlapping spheres and where rearrangements are not as well defined.

The avalanches appear to develop preferentially along shear lines (figure 10). This trend can be understood from the observation of the pattern displayed in figure 6, which shows that the shear-stress variation field induced by a T1 event is highly anisotropic. Although the shear stress is globally relaxed, it is increased in some regions, in particular in the line where the T1 event took place. This increase is likely to trigger further T1 events in the same line and can lead cumulatively to a complete 'unzipping' of the line as illustrated in figure 10.

Because of the disordered nature of the foam, the collective reorganization of the bubbles in the shear band is very different from the standard dislocation motion that controls plasticity in crystalline two-dimensional foams (Bragg & Nye 1947). Figure 10(*c*) shows the location along the shear band of the rearrangements during two consecutive avalanches. Although consecutive T1 events are often nearby, after three to four rearrangements, the location of the plastic events typically moves to another part of the shear band.

We quantitatively analyse this process in the steady-state regime by measuring the spatial correlations of the rearrangements along the flow direction. Figure 11(*a*) shows the coordinate x_i of the ith T1 event as a function of i. The shear band develops after 300 rearrangements (dashed-line). Hereinafter, the probability function $P_k(\Delta x) = \sum_{i=1}^{N} \delta(x_{i+k} - x_i - \Delta x)/N$ is computed (P_k represents the probability for two rearrangements separated by $k-1$ events in the sequence to be located at a distance Δx from each other). The two large peaks of P_1 at $\Delta x = \pm D$ in figure 11(*b*) demonstrate the existence of strong spatial correlations between successive rearrangements. However, this correlation vanishes after about three rearrangements as

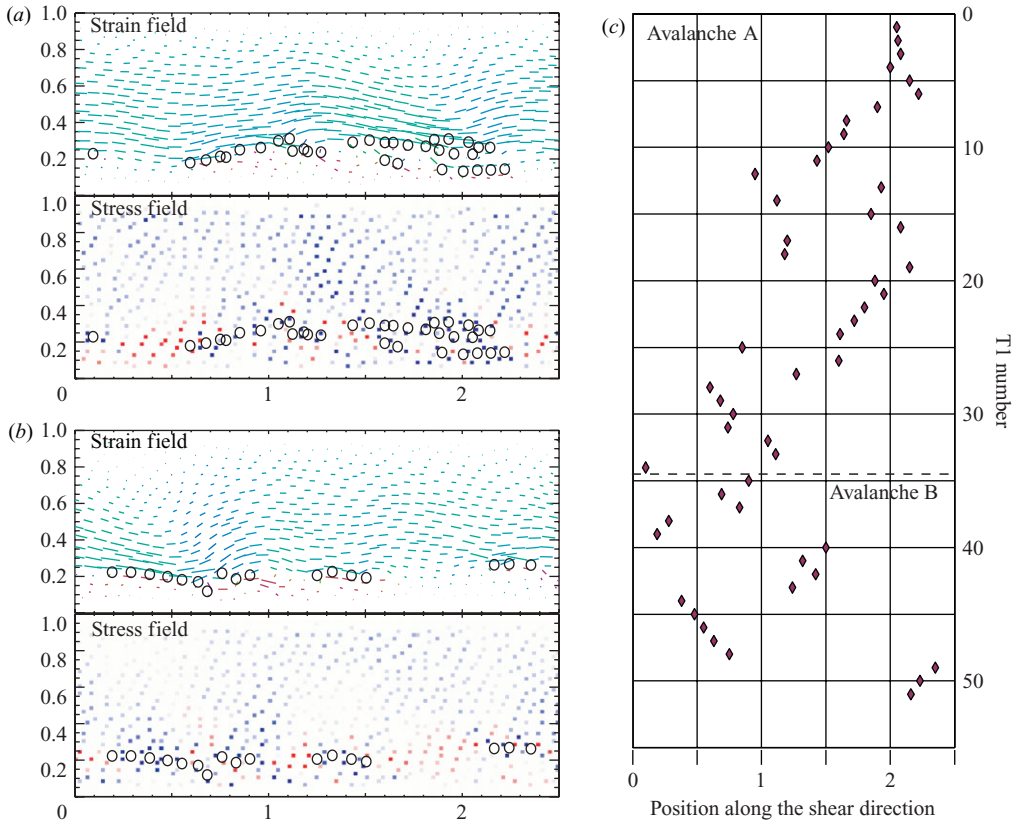

FIGURE 10. (*a*, *b*) Description of two consecutive avalanches in the steady-state regime (numerical simulation). For each one, the displacement and stress fields, resulting from the T1 cascade, are displayed. ○, location of the T1 events involved in the avalanche. (*c*) *x*-coordinate (along the shear band) of the T1 events in chronological order for the two avalanches in (*a*) and (*b*). The dashed line indicates the limit between the two avalanches. This graph illustrates that the second avalanche involves T1 events preferentially located in the region that have not plastically yielded previously. Movies showing the complete sequence of these avalanches are available with the online version of the paper.

indicated by figure 11(*c*) which shows the decay of the spatial correlation as a function of the difference in the indices of the two T1 events.

5. The shear-banding instability

The previous section showed that the peculiar form of the stress propagator associated with a T1 event can account for the appearance of fracture-like processes orientated along the shear direction. This is a first step toward the understanding of the shear-banding instability. However, it does not explain why consecutive avalanches take place in the same region of the foam so that the shear-band is stable in the long run. In the experiment, this could be due to the decay of the mean shear stress across the gap inherent to the Couette geometry, which would maintain the shear band in the region of higher stress near the inner cylinder. However, the numerical study establishes that the same process occurs in plane-parallel shearing geometry in which the shear stress is homogeneous across the gap.

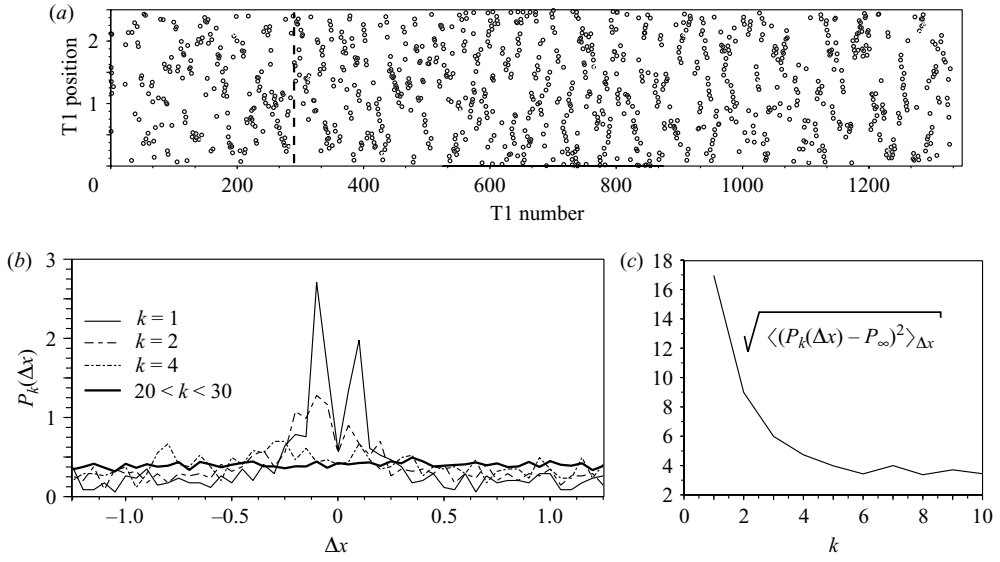

FIGURE 11. (*a*) Position x_i of the rearrangements along the shear direction, as a function of the index i of the rearrangement in the sequence (i is the total number of rearrangements that have occurred since the beginning of the simulation). (*b*) Probability function $P_k(\Delta x)$ (see text) for different values of k. The thick solid line corresponds to $\sum_{20\leqslant k<30} P_k(\Delta x)/10$. At long time scale, $P_k(\Delta x)$ is constant, with a value $P_\infty = 1/L_y$. (*c*) Deviation from the uncorrelated statistics, as a function of the difference k in the indexes of the two T1 events.

The stability of the shear band over time suggests that the shear-banding process is associated with the development of structural heterogeneities which remain permanently imprinted in the foam. In order to test this hypothesis, we attempt to identify local quantities that may differ in the shear band as compared with the rest of the material. In contrast with many studies based on topological measurements (the so-called μ_2 parameter for instance (Weaire & Kermode 1983; Abd el Kader & Earnshaw 1999; Weaire Hutzler 1999), here we focus on energetic and mechanical parameters. This approach aims at offering a more generic framework which may be extended to other disordered systems.

5.1. *Spatial fluctuations of the static stress field*

The disordered nature of the foam structure results in spatial heterogeneities of the static stress field. To characterize these fluctuations, we evaluate, for each bubble of index i at time t, the quantity:

$$\delta_s\sigma_i(t) = \sigma_i(t) - \overline{\sigma}(y, t), \tag{5.1}$$

where $\sigma_i(t)$ is the bubble shear stress and $\overline{\sigma}(y, t)$ is the mean shear stress in the corresponding line. (The indices xy are ignored in the notation of the shear stress, but only this component is considered. The index s stands for static stress fluctuations, as opposed to the dynamic stress fluctuations studied in the next section.) Figure 12 shows the statistical distributions of $\delta_s\sigma(i)$ (notated SSD for static stress distribution), normalized by $\overline{\sigma}(y, t)$, in both the experiment and the numerical simulation. These graphs, obtained from two distinct regions of the foam, show that the SSDs are wider at the location of the shear band than in distant regions. To quantitatively probe the evolution of this characteristic of the stress field, we monitor, for different regions of

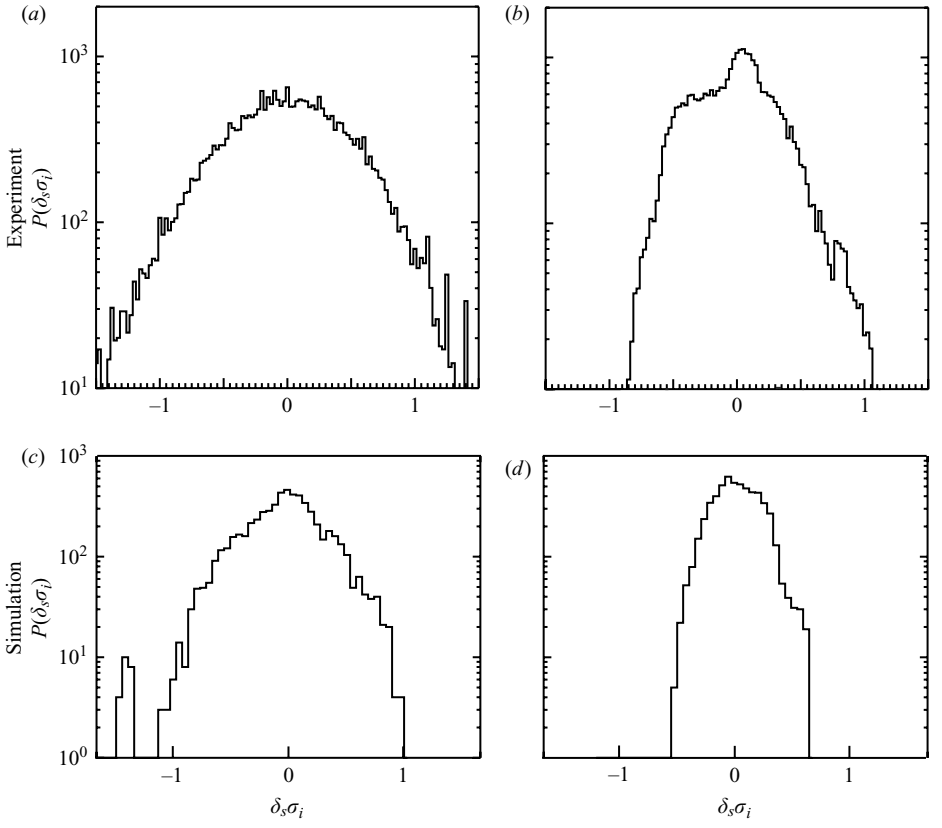

FIGURE 12. Distribution of the bubble shear stress deviation $\delta_s\sigma(i)$ to the local mean value (a, b) in the experiment and (c, d) in the simulation, in the steady-state regime. Two different regions are analysed: (a, c) the shear band, and (b, d) a region located 10 bubble diameters away from the shear band. The regions correspond to strips of width 1 bubble diameter in the experiment, and 2 bubble diameters in the simulation. In order to compare numerical and experimental data, shear stress values have been scaled with respect to the mean shear stress in the steady-state regime.

the sample, the variance of the SSD notated $\Delta_s\sigma^2$ which is defined as:

$$\Delta_s\sigma^2(t) = \frac{\sum_i a_i \delta_s\sigma_i^2(t)}{\sum_i a_i}, \tag{5.2}$$

where a_i is the area of the bubble i. Figure 13(a) shows, in the case of the simulation, the evolution of $\Delta_s\sigma^2$ in three non-overlapping regions of the sample. A similar decrease of the three SSD widths is first observed for an imposed strain lower than 0.5. At the onset of shear banding, the variance of the SSD significantly increases in the shear-band region (square symbols), whereas it remains constant in the rest of the material.

Another characteristic of the foam was previously introduced, the structural energy E_0, defined as the total film-length measured under zero shear stress (it is also the minimum energy of the foam for a given topology and boundary conditions). It is found to increase rapidly at the entrance of the localized regime (figure 5). Figure 13(b)

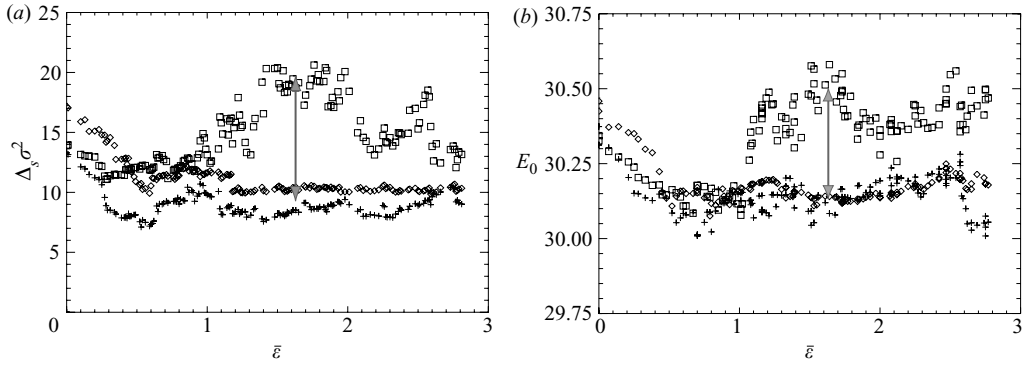

FIGURE 13. Evolution of (*a*) the variance $\Delta_s\sigma^2$ of the static stress distribution (SSD) and (*b*) the structural energy E_0 for three different layers of the foam (simulation). The layers correspond to strips of width 5 bubble diameters. □, shear-band region; ◇, neighbourhood of the opposite wall; +, the middle of the foam. The arrows indicate the maximum amplitudes of variation of both quantities used to test (5.5).

shows the evolution of E_0 obtained from the three sub-regions described before. E_0 exhibits a behaviour qualitatively similar to that observed for the SSD variance.

A simple picture can clarify the physical link between both quantities: consider a macroscopic region of the material submitted to an average shear stress $\overline{\sigma}$. Assuming that all bubbles have the same typical area a and a shear modulus μ, the energy $E(\overline{\sigma})$ of the region can be written as:

$$E(\overline{\sigma}) = \sum_i \left(e_0 + a\frac{\sigma_i^2}{2\,\mu} \right), \tag{5.3}$$

with N being the total number of bubbles, and $A = Na$ the region area. $E(\overline{\sigma})$ can also be rewritten as:

$$E(\overline{\sigma}) = Ne_0 + A\frac{\langle \delta_s\sigma_i^2 \rangle_i}{2\,\mu} + A\frac{\overline{\sigma}^2}{2\,\mu}. \tag{5.4}$$

Therefore, the structural energy $E_0 = E(\overline{\sigma} = 0)$, as a function of the variance of the SSD, is

$$E_0 = Ne_0 + A\frac{\Delta_s\sigma^2}{2\,\mu}. \tag{5.5}$$

From figure 13(*a*), it appears that the maximum amplitudes of variation of $\Delta_s\sigma^2$ and E_0, obtained numerically during a shear experiment, are, respectively, of the order of 10 and 0.4, with a subregion area $A = 0.75$. From (5.5), this yields an expected value for μ of the order of 10, in good agreement with the numerical measurements.

5.2. *A simple scenario for the shear-banding instability*

It has been shown that the transition to shear banding is associated with the development of stress heterogeneities in the shear band, which can be estimated by measuring either E_0 or $\Delta\sigma^2$. As the stress distribution widens, the probability of finding clusters of bubbles submitted to a much larger stress than the average is increased. These sites are more likely to plastically yield in response to a stress increment. It is therefore reasonable to associate the widening of the stress distribution with a decrease in the local yield stress. (Beyond this qualitative description, there is no obvious way to define a local threshold for plasticity in disordered foams.)

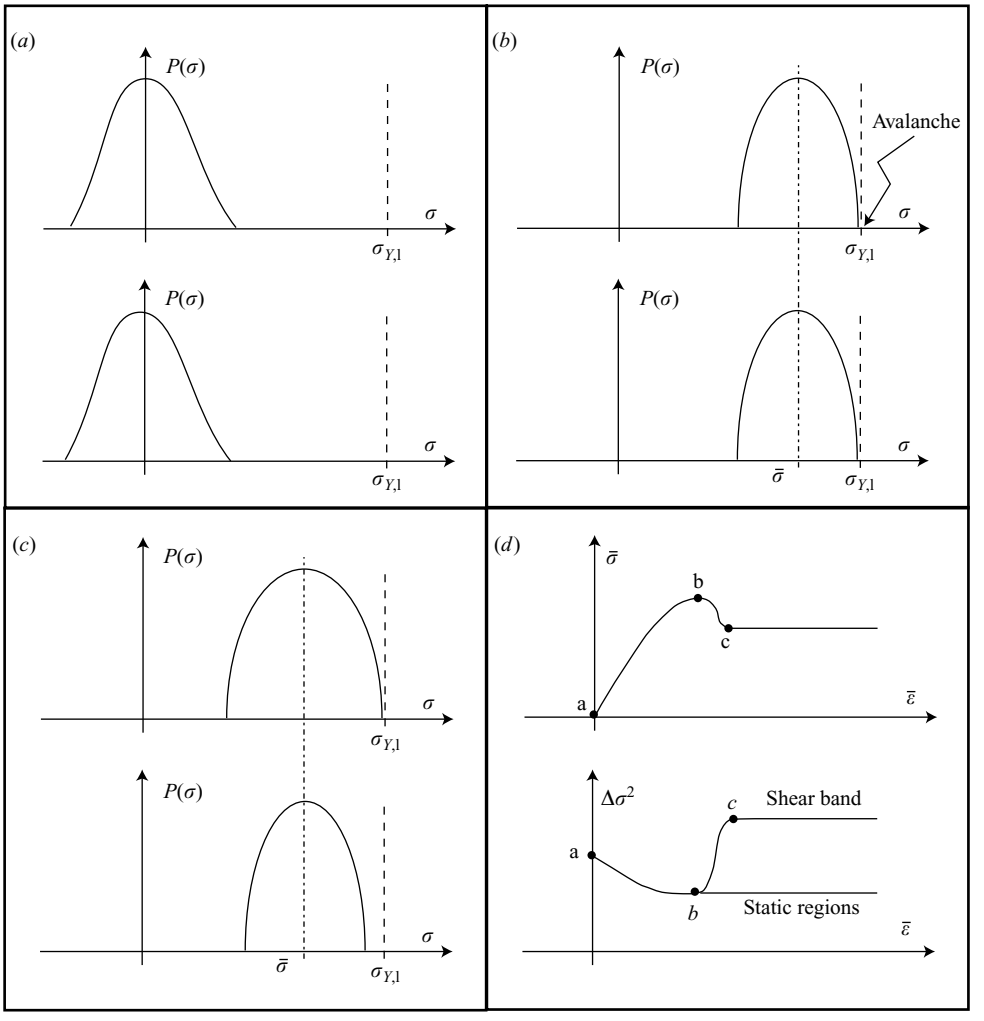

FIGURE 14. Scenario for the shear-banding instability. (*a–c*) The stress distributions in two distinct regions of the foam, at three different times: (*a*) beginning of the experiment: the 'fresh' foam stress field is homogeneous, (*b*) at the onset of shear-banding: a T1 event which triggers an avalanche of rearrangements and enlarges the stress distribution, (*c*) in the steady-state regime: the region where the stress distribution is wider has a lower yield stress. It experiences most of the T1 events. (*d*) The typical evolution of $\overline{\sigma}$, and of $\Delta\sigma^2$ in the two regions. As the shear band develops, the yield stress decreases which results in the observed overshoot of the stress versus strain curve.

Under this hypothesis, a qualitative scenario for the shear-banding instability can be proposed, based on the evolution of the local stress distributions illustrated in figure 14. Let us consider two distinct regions of the foam whose stress distributions are initially assumed to be similar (figure 14*a*). The initial shearing anneals a few structural defects as described in Part 1. The mean shear stress increases until a large fraction of the foam is at the threshold of plastic yielding (figure 14*b*). In this critical state, a T1 event may trigger an avalanche which breaks the symmetry of the system by locally enlarging the static stress distribution (figure 10*a*). A limited region of the foam now has a lower yield stress and is therefore more likely to experience further

plastic events. This description is in many regards similar to the approach proposed by Bulatov & Argon (1994*a*, *b*) in their pioneering work on disordered systems at low temperature. It offers a simple way of understanding the overshoot of the stress versus strain relationship, observed in a wide range of systems (Khan *et al.* 1988; Losert *et al.* 2000).

6. Dynamic stress fluctuations

The previous scenario is based on the observation that plastic events induce both global stress relaxation and local stress heterogeneities. Such a distinction should, however, be refined: T1 events also produce stress heterogeneities far from their location, as depicted on figures 3 and 6. In this section, we describe in more detail the dynamical properties of the stress fluctuations in the continuous flow regime induced by the consecutive T1 events.

6.1. *Dynamics of stress fluctuations*

We evaluate, for each bubble i, time t and time-interval Δt, the dynamic stress fluctuation (see (5.1)):

$$\delta_d\sigma_i(t, \Delta t) = \delta_s\sigma_i(t + \Delta t) - \delta_s\sigma_i(t). \tag{6.1}$$

Figure 15 shows the resulting dynamic stress fluctuation distributions (DSFD) along with the static stress distributions (SSD), obtained from the experiment at increasing distances from the inner edge. The DSFD have been evaluated for a time interval $\Delta t = \tau_0$ corresponding to a wall displacement of 1 bubble diameter. Two situations can be distinguished. In the first three layers of bubbles, the SSD and the DSFD are almost identical and exhibit a remarkable Gaussian shape. This similarity indicates that the static stress field is entirely renewed within a time interval smaller than τ_0. To use an analogy, the system is thermalized within this period of time. For increasing distances from the wheel edge, the width of the DSFD monotonically decreases and becomes significantly smaller than the width of the SSD. In these lines distant from the shear band, the stress fluctuations are insufficient to renew the frozen stress field and the system is mechanically quenched. (Janiaud & Graner (2005) have studied the time fluctuations of the texture tensor on our data. This tensor is found to vary linearly with the stress tensor. Consistently, they observed that the distribution of the fluctuations of this quantity is larger in the shear-band region than in the rest of the material.)

To obtain a more quantitative insight into the DSFD properties, its variance is measured for all time lapses Δt and lines y:

$$\Delta_d\sigma^2(y, \Delta t) = \left\langle \delta_d\sigma_i^2(t, \Delta t) \right\rangle_{\text{bubbles within } \{y \pm \delta y\}, t}. \tag{6.2}$$

Figure 16(*a*) shows the evolution of $\Delta_d\sigma^2(y, \Delta t)$ with increasing time intervals Δt, obtained from the experiment. It exhibits a quasi-diffusive behaviour (with an exponent of the order of 0.8 for the first few lines) for $\Delta t < \tau_0$, and reaches a plateau at longer time. The transition time between these two regimes is an increasing function of the distance to the shearing edge. As shown in figure 16(*b*), the short time-scale diffusion constant decays exponentially with y in the vicinity of the shear band, whereas at larger distances, it exhibits a much slower decay.

6.2. *Stochastic model*

In order to understand these observations, a semi-quantitative stochastic model is developed in this section which aims to relate the dynamics of stress fluctuations to

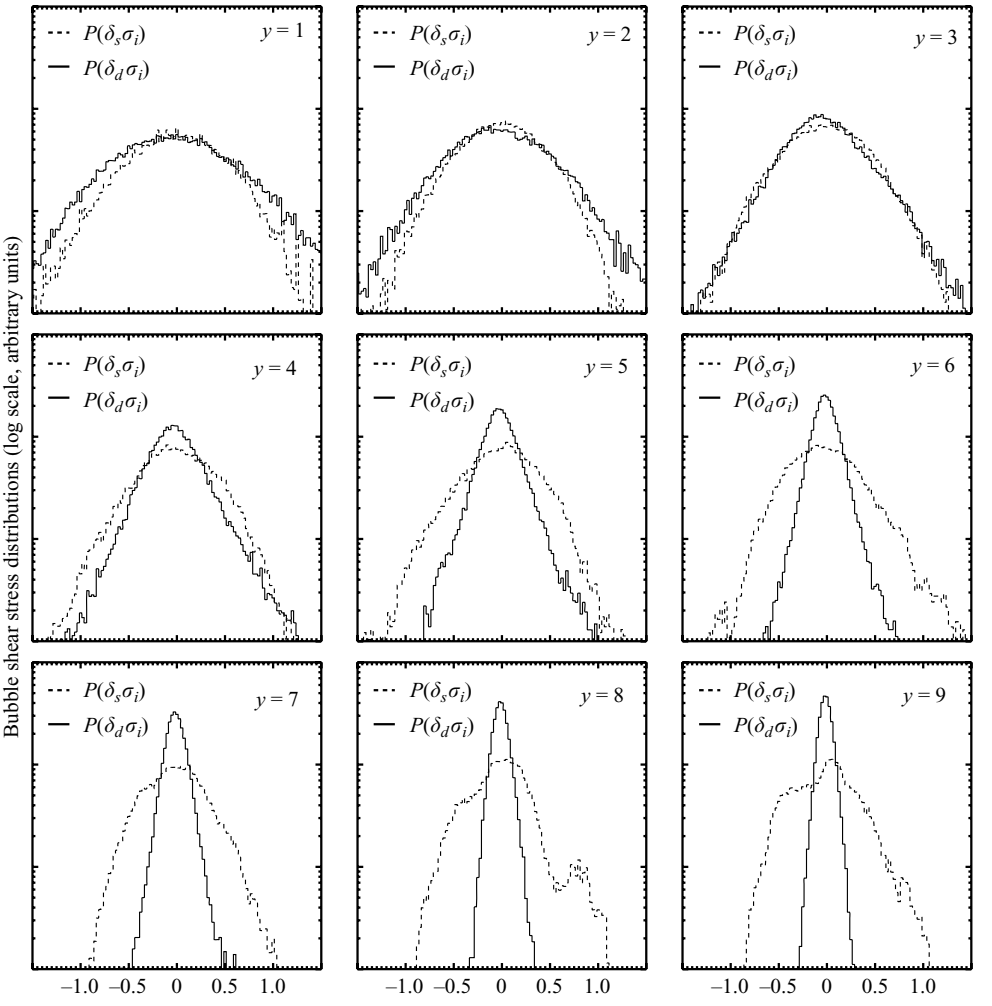

FIGURE 15. Static stress distributions $P(\delta_s\sigma_i)$ and dynamic stress distribution $P(\delta_d\sigma_i(\Delta t))$ measured in the steady-state regime for $\Delta t = \tau_0$ at different distances from the inner wall. Data are obtained from the experiment in the steady-state regime.

the statistical properties of the T1 events. For simplicity, all T1 events are assumed to produce the same stress relaxation (we thus ignore statistical deviations induced by the foam polydispersity which are found to be of the order of 30% in the simulation). We use the analytical results of Picard *et al.* (2004) who calculated the elastic propagator associated with a discrete plastic event in a two-dimensional elastic system, to describe the elastic perturbation induced by each T1 event. Ignoring the effect of boundaries on the stress fluctuations, the elastic propagator associated with a T1 event located at the origin is thus, in polar coordinates (r, θ) (θ being measured from the shearing x-axis):

$$G(r,\theta) = \mu\delta\epsilon_{T1} + G_0(r,\theta) \quad \text{with} \quad G_0(r,\theta) = \delta\sigma_0 D^2 \frac{2\cos(4\theta)}{\pi r^2}. \tag{6.3}$$

The first term in G corresponds to the homogeneous strain relaxation induced by the plastic event, whose maximum amplitude ε_{T1} depends on the system size (see (4.3)). In the fluctuation term G_0, $\delta\sigma_0$ is the stress variation associated with the local plastic

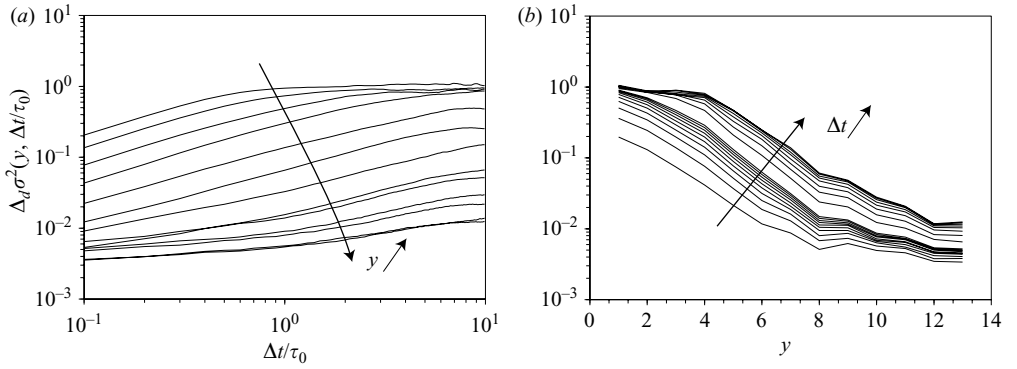

FIGURE 16. Variance of the dynamic stress fluctuations distribution (DSFD) (*a*) as a function of Δt for increasing distances y from the inner wheel (each curve corresponds to a line of width 1 bubble diameter), and (*b*) as a function of y for different $\Delta t/\tau_0$ (from 0.1 to 1, every 0.1, and from 1 to 10, every 1). These results are obtained from the experiment in the steady-state regime.

strain $\varepsilon_{T_1}^{local} \sim 1$, so that $\delta\sigma_0 \sim \mu$. The functional form of G_0 exhibits the quadrupolar symmetry observed in the simulation with a $1/r^2$ decay.

6.2.1. *T1 Statistics*

In order to characterize the spatio-temporal statistics of the T1 events, we introduce the density function $f(x, y, t)$ defined as:

$$f(x, y, t) = \sum_i \delta(x - x_i)\delta(y - y_i)\delta(t - t_i), \tag{6.4}$$

where (x_i, y_i, t_i) are the coordinates in space and time of the T1 events (hereinafter, all spatial coordinates are expressed in units of bubble diameter D). It has been shown in § 4.2 that spatial correlations between rearrangements vanish after two to three T1 events. As we will consider longer time scales, we assume here that T1 events are completely uncorrelated in space and time. This results in the following statistical property for the T1 events density function:

$$\langle f(x, y, t) f(x + \Delta x, y, t')\rangle_{x,t} = \tau^{-1}(y)\ \delta(\Delta x)\ \delta(t - t') \tag{6.5}$$

where $\tau^{-1}(y) = \langle f(x, y, t)\rangle_{x,t} = \partial v(y)/\partial y$ is both the line-averaged T1 frequency and the local strain-rate (equation (4.8)). (This approach is formally analogous to standard stochastic descriptions of surface growth by molecules adsorption (Barabasi & Stanley 1995) which allows us to describe the evolution of interface roughness as a function of the number of adsorbed molecules. Here we seek to relate the 'roughness' of f, i.e. the evolution of the spatial heterogeneities in the number of T1 events per site.) The function $\delta(\Delta x)$ corresponds implicitly to the two-dimensional delta function.

The time-integrated density function

$$\rho(x, y, t, \Delta t) = \int_{t'=t}^{t+\Delta t} f(x, y, t')\,\mathrm{d}t'$$

is further introduced. This function, which measures the number of T1 events that occur between t and $t + \Delta t$ at location (x, y), may be decomposed into a mean and

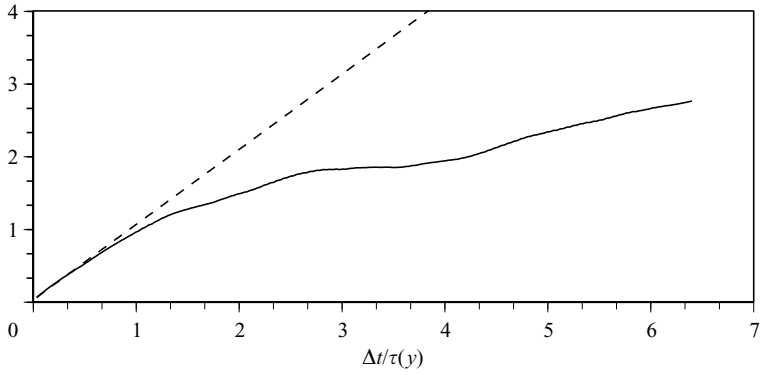

FIGURE 17. (*a*) Evolution of $\langle \rho(x, y, t, \Delta t)\rangle_{x,t}$ (dashed line) and $\langle \delta\rho(x, y, t, \Delta t)^2\rangle_{x,t}$ (solid line) calculated from the T1 events located within a 1 bubble diameter wide strip in the shear band, in the steady-state regime (simulation).

a fluctuating term:

$$\rho(x, y, t, \Delta t) = \tau^{-1}(y)\Delta t + \delta\rho(x, y, t, \Delta t). \tag{6.6}$$

A uniform distribution of (identical) T1 events has no effect on the shear stress fluctuations, and only leads to a homogeneous relaxation of the mean shear stress. Therefore, the stress fluctuations are controlled by the statistical properties of $\delta\rho$. Since rearrangements are assumed to be uncorrelated in space and time, the function ρ follows Poisson statistics with the characteristic property that the variance $\langle \delta\rho^2\rangle_{x,t}$ is equal to the mean $\langle \rho\rangle_{x,t}$ (Grimmett & Stirzaker 2001). This leads to the following autocorrelation function for $\delta\rho$:

$$\langle \delta\rho(x, y, t, \Delta t)\delta\rho(x + \Delta x, y, t, \Delta t)\rangle_{x,t} = \tau^{-1}(y)\Delta t\delta(\Delta x). \tag{6.7}$$

In order to test the validity of this relation, the function ρ is evaluated in the simulation by monitoring, at each site (x, y), the T1 events located within a distance $D/2$. Figure 17(*a*) shows, for a line of width 1 bubble diameter in the shear band, the evolution of the mean number of T1 events per site $\langle \rho(x, y, t, \Delta t)\rangle_{x,t}$ (dashed line), and the mean square deviation $\langle \delta\rho^2(x, y, t, \Delta t)\rangle_{x,t}$ (solid line) as a function of Δt. On short time scales, $\langle \delta\rho^2\rangle_{x,t}$ and $\langle \rho\rangle_{x,t}$ exhibit a similar linear increase with Δt in agreement with (6.7). For $\Delta t \geqslant \tau(y)$, however, $\langle \delta\rho^2(\Delta t)\rangle_{x,t}$ becomes significantly smaller than $\langle \rho\rangle_{x,t}$. This second regime indicates that the hypothesis of Markovian statistics for the T1 events sequence is incorrect for integration times Δt larger than $\tau(y)$; the locations of the T1 events that occur between t and $t + \Delta t$ depend on the sequence of T1 events that occurred previously in a way which limit the amplitudes of variation of $\delta\rho$.

This effect is directly visible on figure 10(*c*) which shows that, in a sequence of two consecutive avalanches, the second one involves T1 events preferentially in the regions that have not plastically yielded during the first one. This long time-scale statistical bias can be qualitatively understood through a simple argument. If the sequence of T1 events were completely stochastic, this would lead to stress fluctuations of infinite amplitude, which is incompatible with the existence of a finite yield stress. Conversely, a constraint of finite stress fluctuations would impose a bound on $\delta\rho^2$ if all rearrangements produced the same stress perturbation. However, any dispersion in the values of the stress $\delta\sigma_0$, released by the T1 events, allows for a slow diffusive increase of $\delta\rho^2$ as observed in figure 17 at large Δt.

In our attempt to model the stress dynamics, we assumed that all the events produce a similar effect ($\delta\sigma_0$ is single valued). Consistently, $\langle\delta\rho^2\rangle$ must be bounded. We thus explicitly impose a maximum deviation in the total number of T1 events per site equal to 1 reached after a time $\tau(y)$ and modify (6.7) accordingly:

$$\langle\delta\rho(x, y, t, \Delta t)\delta\rho(x + \Delta x, y, t, \Delta t)\rangle_{x,t} = \left(1 - \exp\left(-\frac{\Delta t}{\tau(y_p)}\right)\right)\delta(\Delta x) \tag{6.8}$$

6.2.2. *Shear stress fluctuations*

Having described the statistics of the T1 events, we now seek to evaluate the stress fluctuations that they induce on a given line y. Based on (6.3) and (6.8), the variance of the DSFD of line y originating from T1 events taking place in line y_p can be written as:

$$\begin{aligned}
\Delta_d\sigma^2_{y_p\to y}(\Delta t) &= \left\langle \left(\int_{x'} \rho(x', y, t, \Delta t)G_0(x - x', y - y_p)\,\mathrm{d}x'\right)^2\right\rangle_{x,t} \\
&= \int_{X'}\int_{X''} G_0(X', y - y_p)G_0(X'', y - y_p) \\
&\quad \times \langle\rho(x - X', y, t, \Delta t)\rho(x - X'', y, t, \Delta t)\rangle_{x,t}\,\mathrm{d}X'\mathrm{d}X'' \\
&= \int_{X'}\int_{X''} G_0(X', y - y_p)G_0(X'', y - y_p) \\
&\quad \times \langle\delta\rho(x - X', y, t, \Delta t)\delta\rho(x - X'', y, t, \Delta t)\rangle_{x,t}\,\mathrm{d}X'\,\mathrm{d}X'', \\
\Delta_d\sigma^2_{y_p\to y}(\Delta t) &= \frac{\delta\sigma_0^2}{\pi|y - y_p|^3}\left(1 - \exp\left(-\frac{\Delta t}{\tau(y_p)}\right)\right).
\end{aligned} \tag{6.9}$$

This relationship is only valid for $y \neq y_p$. The exact calculation for $y \sim y_p$ would require a detailed description of the plastic process at the bubble scale, which is beyond the scope of the present paper. Instead, we set the value of the elastic cutoff length at 1 (i.e. the bubble diameter) and assume that, for $r < 1$, the stress fluctuation amplitude is uniform and equal to $\delta\sigma_0$. Under this assumption, the previous developments lead to:

$$\Delta_d\sigma^2_{y_p\sim y}(\Delta t) = \delta\sigma_0^2\left(1 - \exp\left(-\frac{\Delta t}{\tau(y_p)}\right)\right). \tag{6.10}$$

Assuming these different sources of fluctuation to be uncorrelated, the variance of the dynamic stress fluctuation distribution at a given line y can then be obtained by integrating (6.9) and (6.10) over y_p:

$$\Delta_d\sigma^2(y, \Delta t) = \int_{y_p} \Delta_d\sigma^2_{y_p\to y}(y, \Delta t)\,\mathrm{d}y_p. \tag{6.11}$$

6.2.3. *Numerical solutions*

This calculation yields a prediction of the statistics of the stress fluctuations in the sheared foam from the knowledge of the strain-rate profile $\tau(y)^{-1}$. In order to test this model against the experiment, we extract $\tau(y)$ from the measured plastic flow profile (figure 2). Since the latter decays exponentially with the distance from the inner wall, with a decay length of the order of 1 bubble diameter, $\tau(y)$ can be estimated as:

$$\tau(y) = \tau_0\ \exp(y). \tag{6.12}$$

Figure 18 shows the characteristics of $\Delta_d\sigma^2(y, \Delta t)$ numerically calculated for a discrete system composed of 20 lines of bubbles ($\delta\sigma_0$ is set at 1). This model accounts

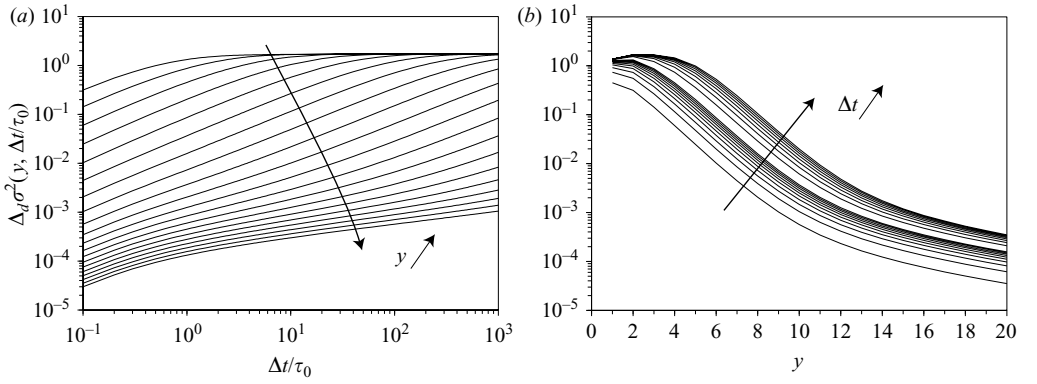

FIGURE 18. Predicted evolution of the variance of the dynamical stress fluctuations distribution (see text for details of the model). The different values for the time intervals Δt and distances y from the shearing wall, are similar to those used in figure 16 to allow for a direct comparison with the experiment.

for several features of its experimental counterpart (figure 16), namely (i) a diffusive regime for $\Delta t < \tau_0$, (ii) a saturation occurring after a time of order $\tau(y)$, (iii) a transition from an exponential decay in the shear band to a power-law decay at larger distance. These two regimes can be associated with two distinct processes. Local plasticity is the main source of stress fluctuation in the layers of bubbles where a large number of T1 events occur, and the resulting stress dynamics is directly connected to the plastic frequency $\tau^{-1}(y)$ of the given line. In contrast, long-range elastic stress fluctuations induced by distant T1 events are dominant for lines with negligible plasticity. (This interpretation is confirmed by the experimental observation that these fluctuations exhibit large length-scale spatial correlations in distant lines, as reported in Debrégeas *et al.* (2001).) The resulting stress fluctuation amplitude decays as a power law with the distance to the shear band.

6.3. *Discussion*

The observation made in this section that the stress fluctuations are not diffusive on long time-scales is due to the fact that the cumulative effect of T1 events in a given line can only produce a finite deformation of the structure in a distant line. As a result, beyond the shear band where a large number of rearrangements are observed, these fluctuations are insufficiently intense to renew the structure (figure 15); their amplitude remains small in comparison to the width of the static stress distribution. The latter, which is mostly set during foam preparation, thus plays a prominent role in fixing the local frequency of T1 events.

Several mean-field models of soft glass rheology are based on empirical equations that relate the stress fluctuation amplitude to the plastic event frequency (Sollich *et al.* 1997; Falk & Langer 1998). They capture many of the features observed in foams at finite shear rate in which fluctuations originating from nearby T1 events are expected to be dominant. As mean field models, these approaches are inadequate to describe correctly the creep flow behaviour for which long-range elastic coupling becomes important. This is done by Baret, Vandembroucq & Roux (2002) and Picard *et al.* (2005) in numerical models which exhibit shear banding. Picard *et al.* use the exact elastic calculation of the shear stress released by a plastic event. Although, in confined geometries, they found that the shear band develops close to the walls, the shear-banding instability is still observed in bi-periodic systems.

7. Conclusion

We showed in Part 1 that when a foam is submitted to an oscillating shear of moderate amplitude (maximum strain less than 0.5), the strain reduces the structural disorder by curing topological defects, thus extending the elastic domain of the material. In this regime, T1 events are uncorrelated in space and time. In contrast, for large amplitude of strain, T1 events occur in the form of fracture-like processes which yield local heterogeneities in the stress field and a reduction of the yield stress. This mechanism is at the base of the shear-banding instability observed in both the simulation and the experiment.

In the steady-state regime, large stress fluctuations are observed even in the region where few plastic events occur. These fluctuations are associated with the long-range elastic relaxation induced by T1 events. A simple statistical model allows us to predict the time evolution of these fluctuations from the knowledge of the time-averaged flow profile. Although the dynamic fluctuations can be estimated regardless of the detailed foam structure, the local T1 event frequency cannot be extracted from the knowledge of the fluctuations alone. The probability for a plastic event to occur depends on both the structural disorder of the system (which yields an effective yield stress), and the fluctuations that allow this threshold to be reached. We therefore believe that the model developed in Debrégeas *et al.* (2001), which was based on dynamical fluctuations alone, was incomplete. Further work is necessary to provide a complete picture of the coupled dynamic between stress fluctuations and plasticity in such disordered systems.

Many of these results should remain valid for disordered systems at low temperature provided that there is (i) an elastic response at low strain and (ii) a typical duration of plastic relaxation much shorter than the imposed shearing time scale. The elastic propagator associated with a local plastic event will exhibit the same generic pattern, regardless of the underlying structure (Eshelby 1957; Picard *et al.* 2004). The quadrupolar symmetry of this stress relaxation pattern is at the origin of the fracture-like processes observed in foam and other systems such as Lennard-Jones glasses for instance (Maloney & Lemaitre 2004; Shi & Falk 2005).

The long-range elastic coupling opens the possibility of heterogeneous flows. However, the evolution toward long-lived localization (shear bands) might depend on many specific characteristics of the system. This paper provides one possible explanation which is based on the appearance of large heterogeneities in the stress distributions, induced by the first avalanches of plastic processes. The regions where the stress distributions are widest have a lower effective yield stress, and are thus more likely to experience further plastic processes. This self-amplifying process tends to maintain the plastic events in limited regions of the material. Such a shear-banding process requires a broad enough range of disorder accessible to the system, in order to allow large variations of the local yield stress to pertain. It is clearly not applicable to monodisperse (or even fairly monodisperse) systems, in which the flow is associated with the motion of dislocation as in crystalline solids (Cox *et al.* 2004; Wang *et al.* 2006). The influence of the walls might also be critical since they locally constrain the bubble shapes and thus tend to make the material locally more likely to yield (Howell, Behringer & Veje 1999; Mueth *et al.* 2000; Fenistein & van Hecke 2003). The precise conditions that lead to the shear-banding transition still remain to be clarified.

The experiments on confined foams were initiated with Jean-Marc di Meglio. We wish to thank Guillemette Picard, Christiane Caroli, Olivier Pouliquen and Jean

Rajchenbach for fruitful discussions. We are especially grateful to Christiane Caroli for her careful reading of Part 1.

REFERENCES

Abd el Kader, A. & Earnshaw, J. C. 1999 Shear-induced changes in two-dimensional foam. *Phys. Rev. Lett.* **82**, 2610–2613.

Asipauskas, M., Aubouy, M., Glazier, J. A., Graner, F. & Jiang, Y. 2003 A texture tensor to quantify deformations: the example of two-dimensional flowing foams. *Granular Matter* **5**, 71–74.

Barabási, A.-L. & Stanley, H.-E. 1995 *Fractal Concepts in Surface Growth.* Cambridge University Press.

Baret, J. C., Vandembroucq, D. & Roux, S. 2002 An extremal model for amorphous media plasticity. *Phys. Rev. Lett.* **89**, 195506.

Bragg, L. & Nye, J. F. 1947 A dynamical model of a crystal structure. *Proc. R. Soc. Lond.* A **190**, 474–482.

Bulatov, V. V. & Argon, A. S. 1994*a* A stochastic model for continuum elasto-plastic behavior: I. Numerical approach and strain localization. *Modelling Simul. Mater. Sci. Engng* **2**, 167–184.

Bulatov, V. V. & Argon, A. S. 1994*b* A stochastic model for continuum elasto-plastic behavior: II. A study of the glass transition and structural relaxation. *Modelling Simul. Mater. Sci. Engng* **2**, 185–202.

Bulatov, V. V. & Argon, A. S. 1994*c* A stochastic model for continuum elasto-plastic behavior: III. Plasticity in ordered versus disordered solids. *Modelling Simul. Mater. Sci. Engng* **2**, 203–222.

Cantat, I. & Delannay, R. 2005 Dissipative flows of 2D foams. *Eur. Phys. J.* E **18**, 55–67.

Chen, K., Bak, P. & Obukhov, S. P. 1991 Self-organized criticality in a crack-propagation model of earthquakes. *Phys. Rev.* A **43**, 625.

Clancy, R. J., Janiaud, E., Weaire, D. & Hutzler, S. 2006 The response of 2D foams to continuous applied shear in a Couette rheometer. *Eur. Phys. J.* E **21**, 123–132.

Cohen-Addad, S., Hohler, R. & Khidas, Y. 2004 Origin of the slow linear viscoelastic response of aqueous foams. *Phys. Rev. Lett.* **93**, 028302-1.

Courty, S., Dollet, B., Elias, F., Heinig, P. & Graner, F. 2003 Two-dimensional shear modulus of a Langmuir foam. *Europhys. Lett.* **64**, 709–715.

Cox, S., Weaire, D. & Glazier, J. A. 2004 The rheology of two-dimensional foams. *Rheol. Acta* **43**, 442–448.

Debrégeas, G., Tabuteau, H. & di Meglio, J.-M. 2001 Deformation and flow of a two-dimensional foam under continuous shear. *Phys. Rev. Lett.* **87**, 178305.

Dennin, M. & Knobler, C. M. 1997 Experimental studies of bubble dynamics in a slowly driven monolayer foam. *Phys. Rev. Lett.* **78**, 2485–2488.

Dollet, B., Elias, F., Quilliet, C., Raufaste, C., Aubouy, M. & Graner, F. 2005 Two-dimensional flow of foam around an obstacle: force measurements. *Phys. Rev.* E **71**, 031403.

Durand, M. & Stone, H. A. 2006 Relaxation time of the topological T1 process in a two-dimensional foam. *Phys. Rev. Lett.* **97**, 226101.

Durian, D. J. 1995 Foam mechanics at the bubble scale. *Phys. Rev. Lett.* **75**, 4780.

Durian, D. J., Weitz, D. A. & Pine, D. J. 1991 Multiple light-scattering probes of foam structure and dynamics. *Science* **252**, 686–688.

Eshelby, J. D. 1957 The determination of the elastic field of an ellipsoidal inclusion and related problems. *Proc. R. Soc. Lond.* A **241**, 376.

Falk, M. L. & Langer, J. S. 1998 Dynamics of viscoplastic deformation in amorphous solids. *Phys. Rev.* E **57**, 7192.

Fenistein, D. & van Hecke, M. 2003 Wide shear zones in granular bulk flow. *Nature* **425**, 256.

Gopal, A. D. & Durain, D. J. 1995 Nonlinear bubble dynamics in a slowly driven foam. *Phys. Rev. Lett.* **75**, 2610–2613

Gopal, A. D. & Durain, D. J. 1999 Shear-induced 'melting' of an aqueous foam. *JCIS* **213**, 169–178.

Grimmett, G. R. & Stirzaker, D. R. 2001 *Probability and Random Processes*, 3rd edn. Oxford University Press.

Hohler, R., Cohen-Addad, S. & Hoballah, H. 1997 Periodic nonlinear bubble motion in aqueous foam under oscillating shear strain. *Phys. Rev. Lett.* **79**, 1154–1157.

Howell, D., Behringer, R. P. & Veje, C. 1999 Stress fluctuations in a 2D granular Couette experiment: a continuous transition. *Phys. Rev. Lett.* **82**, 5241–5244.

Janiaud, E. & Graner, F. 2005 Foam in a two-dimensional Couette shear: a local measurement of bubble deformation. *J. Fluid Mech.* **532**, 243–267.

Janiaud, E., Weaire, D. & Hutzler, S. 2006 Two-dimensional foam rheology with viscous drag. *Phys. Rev. Lett.* **97**, 038302.

Kabla, A. & Debrégeas, G. 2003 Local stress relaxation and shear-banding in a dry foam under shear. *Phys. Rev. Lett.* **90**, 258303.

Kabla, A. & Debrégeas, G. 2007 Quasi-static rheology of foams. Part 1. Oscillating strain. *J. Fluid Mech.* **587**, 23–44.

Khan, S. A., Schnepper, C. A. & Armstrong, R. C. 1988 Foam rheology: III Measurement of shear flow properties. *J. Rheol.* **32**, 69–92.

Kraynik, A. M., Reinelt, D. A. & van Swol, F. 2003 Structure of random monodisperse foam. *Phys. Rev.* E **67**, 031403.

Lauridsen, J., Twardos, M. & Dennin, M. 2002 Shear-induced stress relaxation in a two-dimensional wet foam. *Phys. Rev. Lett.* **89**, 098303.

Losert, W., Géminard, J.-C., Nasuno, S. & Gollub, J. P. 2000 Mechanisms for slow strengthening in granular materials. *Phys. Rev.* E **61**, 4060–4068.

Maloney, C. & Lemaitre, A. 2004 Subextensive scaling in the athermal, quasistatic limit of amorphous matter in plastic shear flow. *Phys. Rev. Lett.* **93**, 016001.

Mueth, D. M., Debrégeas, G., Karczmar, G. S., Eng, P. J., Nagel, S. R. & Jaeger, H. M. 2000 Signatures of granular microstructure in dense shear flows. *Nature* **406**, 385–389.

Okuzono, T. & Kawasaki, K. 1995 Intermittent flow behavior of random foams: a computer experiment on foam rheology. *Phys. Rev.* E **1995**, 1246–1253.

Picard, G., Ajdari, A., Lequeux, F. & Bocquet, L. 2004 Elastic consequences of a single plastic event: a step towards the microscopic modeling of the flow of yield stress fluids. *Eur. Phys. J.* E **15**, 371–381.

Picard, G., Ajdari, A., Lequeux, F. & Bocquet, L. 2005 Slow flows of yield stress fluids: complex spatiotemporal behavior within a simple elastoplastic model. *Phys. Rev.* E **71**, 010501(R).

Pratt, E. & Dennin, M. 2003 Nonlinear stress and fluctuation dynamics of sheared disordered wet foam. *Phys. Rev.* E **67**, 051402.

Rodts, S., Baudez, J. C. & Coussot, P. 2005 From discrete to continuum flow in foams. *Europhys. Lett.* **69**, 636–642.

Shi, Y. & Falk, M. L. 2005 Strain localization and percolation of stable structure in amorphous solids. *Phys. Rev. Lett.* **95**, 095502.

Sollich, P., Lequeux, F., Hébraud, P. & Cates, M. E. 1997 Rheology of soft glassy materials. *Phys. Rev. Lett.* **78**, 2020.

Tewari, S., Schiemann, D., Durian, D. J., Knobler, C. M., Langer, S. A. & Liu, A. J. 1999 Statistics of shear-induced rearrangements in a two-dimensional model foam. *Phys. Rev.* E **60**, 4385–4396.

Varnik, F., Bocquet, L., Barrat, J.-L. & Berthier, L. 2003 Shear localization in a model glass. *Phys. Rev. Lett.* **90**, 095702.

Wang, Y., Krishan, K. & Dennin, M. 2006 Impact of boundaries on the velocity profiles in bubble rafts. *Phys. Rev.* E **73**, 031401.

Weaire, D. & Hutzler, S. 1999 *The Physics of Foams.* Clarendon Press, Oxford.

Weaire, D. & Kermode, J. P. 1983 Computer simulation of a two-dimensional soap froth I. Method and motivation. *Phil. Mag.* B **48**, 245–259.